



ELSEVIER



Nanomedicine: Nanotechnology, Biology, and Medicine  
37 (2021) 102448



nanomedjournal.com

# PROKR1 delivery by cell-derived vesicles restores the myogenic potential of *Prokr1*-deficient C2C12 myoblasts<sup>\*\*\*</sup>

Chunjuan Zhang, MSc<sup>a</sup>, Jongsoo Mok, MSc<sup>b</sup>, Yeonwoo Seong, Ms<sup>a</sup>, Hui-chong Lau, PhD<sup>c</sup>,  
Dayeon Kim, MSc<sup>c</sup>, Junsik Yoon, MSc<sup>c</sup>, Seung Wook Oh, PhD<sup>c</sup>, Tae Sub Park, PhD<sup>a,b</sup>,  
Joonghoon Park, PhD<sup>a,b,\*</sup>

<sup>a</sup>Department of International Agricultural Technology, Graduate School of International Agricultural Technology, Seoul National University, Republic of Korea

<sup>b</sup>Institute of GreenBio Science and Technology, Seoul National University, Republic of Korea

<sup>c</sup>Biodrone Research Institute, MDimune Inc., Republic of Korea

Revised 11 June 2021

## Abstract

Cell-derived vesicles (CDVs) have been investigated as an alternative to exosomes. Here, we generated CDVs from Prokineticin receptor 1 (*PROKR1*) overexpressing HEK293T cells using micro-extrusion. More than 60 billion *PROKR1*-enriched CDV (*PROKR1*<sup>Tg</sup> CDVs) particles with canonical exosome properties were recovered from 10<sup>7</sup> cells. With 25 μg/mL of *PROKR1*<sup>Tg</sup> CDVs, we observed delivery of *PROKR1*, significant reduction of apoptosis, and myotube formation in C2C12<sup>*Prokr1*<sup>-/-</sup></sup> myoblasts that have lost their myogenic potential but underwent apoptosis following myogenic commitment. Expression levels of early and late myogenic marker genes and glucose uptake capacity were restored to equivalent levels with wild-type control. Furthermore, *PROKR1*<sup>Tg</sup> CDVs were accumulated in soleus muscle comparable to the liver without significant differences. Therefore, CDVs obtained from genetically engineered cells appear to be an effective method of *PROKR1* protein delivery and offer promise as an alternative therapy for muscular dystrophy.

© 2021 The Author(s). Published by Elsevier Inc. This is an open access article under the CC BY-NC-ND license (<http://creativecommons.org/licenses/by-nc-nd/4.0/>).

**Key words:** Cell-derived vesicles; *PROKR1*; C2C12; Myogenesis; Muscular dystrophy

Exosomes are vesicles that bud from multicellular organisms for intercellular communication.<sup>1</sup> They transport various biomolecules between cells, including proteins, lipids, mRNA, microRNAs, and DNA, and are of great interest for diagnostics and drug delivery due to their excellent biodistribution and biocompatibility.<sup>2,3</sup>

Over the past 10 years, significant progress has been made in exosome isolation and purification techniques, and these advances have led to encouraging achievements in the field of exosome biology. Exosome isolation is achieved primarily via three different techniques. Ultracentrifugation is generally considered the gold

standard for exosome isolation, although this process is labor-intensive and has the drawback of contamination with the cell-derived proteins and lipoproteins often found in isolated exosomes.<sup>4</sup> Ultrafiltration and size-exclusion chromatography are size-based exosome isolation techniques using membrane filters with defined molecular weight or size exclusion limits. These methods are faster than ultracentrifugation; however, they are difficult to scale up and the deformation or destruction of vesicles that occurs during the filtration process can distort the results of downstream experiments.<sup>5</sup> Immunoaffinity capture exploits the interactions

Statement disclosing any commercial associations: There is no conflict of interest.

Acknowledgment: This work was supported by Korea Health Industry Development Institute, the Ministry of Health and Welfare (KHIDI-HI14C1135) and National Research Foundation (NRF-2018R1D1A1B07048516).

Competing interests: The authors declare no competing financial interest.

Data availability: No datasets were generated or analyzed during the current study.

\* Corresponding author at: Department of International Agricultural Technology, Graduate School of International Agricultural Technology, Seoul National University, Republic of Korea.

E-mail address: [joonghoon@snu.ac.kr](mailto:joonghoon@snu.ac.kr) (J. Park).

<https://doi.org/10.1016/j.nano.2021.102448>

1549-9634/© 2021 The Author(s). Published by Elsevier Inc. This is an open access article under the CC BY-NC-ND license (<http://creativecommons.org/>)

between exosomal membrane proteins and their dedicated antibodies; this method is highly effective for the selective isolation of pure exosomes. However, the lack of effective exosomal marker proteins and low exosome isolation yields have limited the use of this technique.<sup>4</sup> Despite advances in exosome isolation and purification, these techniques are not ready for clinical implementation as they are hindered by limitations in terms of exosome purity, scalability, validation, and standardization.<sup>6–8</sup> While the selective production of exosomes containing active pharmaceutical biomolecules is the primary objective of all types of nanovesicle-based drug delivery systems, conventional exosome isolation techniques have not yet been met this goal.

To address these issues, an alternative method, with high yield and reproducibility, for generating exosome-mimetic nanovesicles enriched with the target molecule of interest has been investigated. Cell-derived vesicles (CDVs), which are exosome-mimetic nanovesicles that can be prepared by micro-extrusion of source cells, present many similarities to exosomes in terms of size, morphology, and the molecular composition of membranes.<sup>7,9</sup> CDVs have been shown to deliver cellular information to recipient cells and to induce biological responses. For example, CDVs produced from hepatocytes successfully promoted hepatocyte proliferation and liver regeneration by delivering hepatocyte-specific proteins.<sup>10</sup> CDVs can be loaded with exogenous pharmaceutical molecules via electroporation or extrusion from the cell type of choice<sup>9,11</sup>; this represents an advantage over exosomes, which require selective sorting of cargo by genetic control of endosomal pathways.<sup>12</sup> CDVs also exhibit natural targeting ability, maintaining the topology of plasma membrane proteins.<sup>12</sup> For example, membrane proteins present on the surface of CDVs derived from cancer cells have been shown to be critical for the efficient delivery of doxorubicin; after delivery into cells, doxorubicin-enriched CDVs alter cell signaling and induce superior anti-cancer effects compared to doxorubicin alone.<sup>9</sup> Therefore, CDVs are regarded as an alternative to exosomes due to their high yield and productivity, and may be an efficient drug delivery system for active pharmaceutical biomolecules.

Muscular dystrophy that occurs with age, also known as sarcopenia, is a significant public health issue.<sup>13</sup> Sarcopenia has been linked to increased morbidity and metabolic malfunction, and is characterized by features including loss of muscle mass, altered muscle composition, fat and fibrous tissue infiltration, and alterations in innervation.<sup>14</sup> A better understanding of the pathophysiology of sarcopenia will aid in the development of strategies mitigating the impact of its adverse effects; however, most pharmacological agents investigated to date are hormonal and myostatin modulators designed to increase muscle mass.<sup>15</sup> Prokineticin receptor 1 (*Prokr1*) is a G protein-coupled receptor that participates in metabolic functions, especially in peripheral tissues such as fat, blood vessels, and the heart.<sup>16</sup> For example, *Prokr1* suppresses adipocyte proliferation and differentiation, and is downregulated in the fat tissue of obese patients.<sup>17</sup> *Prokr1* also simulates the capillary development of endothelial cells and insulin-stimulated glucose uptake,<sup>18</sup> as well as cardiomyocyte ventricular activity, by promoting angiogenesis.<sup>19</sup> Although analysis of tissue distribution has revealed the expression of

*Prokr1* in skeletal muscle,<sup>20,21</sup> the myogenic function of *Prokr1* has not yet been investigated.

In this study, we generated *Prokr1*-deficient C2C12 (C2C12-*Prokr1*<sup>-/-</sup>) murine myoblasts, which showed loss of myogenic potential and underwent apoptosis after myogenic commitment. We then prepared PROKR1-enriched CDVs from *PROKR1*-overexpressing (*PROKR1*<sup>Tg</sup>) HEK293T cells. When we applied the PROKR1-enriched CDVs to C2C12-*Prokr1*<sup>-/-</sup> myoblasts, the CDVs successfully delivered the PROKR1 protein to C2C12-*Prokr1*<sup>-/-</sup> myoblasts, reduced apoptotic cell death after myogenic commitment, and rescued the morphological and functional development of myotubes. Therefore, CDVs obtained from genetically engineered cells appear to be an effective method of delivery of PROKR1 protein and offer promise as an alternative therapy for muscular dystrophy.

## Methods

### Generation of genetically engineered cells

Human embryonic kidney 293T (HEK293T) and mouse C2C12 myoblasts were purchased from American type culture collection (ATCC, Manassas, VA, USA). To establish the *PROKR1* transgenic HEK293T cells (*PROKR1*<sup>Tg</sup> HEK293T), piggyBac cloning and expression vector containing *PROKR1* cDNA was co-transfected with transposon (Systems Biosciences, Palo Alto, CA, USA) using Lipofectamine 3000 (Invitrogen, Carlsbad, VA, USA) according to the manufacturer's protocol. To knock out the *PROKR1* gene in HEK293T (HEK293T-*PROKR1*<sup>-/-</sup>) and C2C12 cells (C2C12-*Prokr1*<sup>-/-</sup>), pUC57 expression vector containing guide RNA (gRNA) was co-transfected with Cas9 protein using Lipofectamine 3000 according to the manufacturer's instructions.

### Cell maintenance and differentiation

HEK293T cells were cultured in 4.5 g/L DMEM media (Gibco, Grand Island, NY, USA) supplemented with 10% (v/v) exosome-free fetal bovine serum (FBS, Gibco) and 1% antibiotic-antimycotic (Gibco, Grand Island, NY, USA) which were incubated at 37 °C in 5% CO<sub>2</sub>. C2C12 cells were maintained in 1 g/L D-glucose DMEM (Gibco) supplemented with 20% (v/v) exosome-free FBS and 1% antibiotic-antimycotic (Gibco). For differentiation, 1 × 10<sup>6</sup> C2C12 cells were seeded, and after reaching 90% confluence, cells were subjected to differentiation in 4.5 g/L DMEM with 2% horse serum (Gibco) for 6 days.

### Generation and purification of CDVs

HEK293T cell-derived vesicles (CDVs) were generated by using a micro-extruder (Avanti Polar Lipids, Inc., Alabaster, Alabama, USA) (Supplementary Figure 1, A). The cell suspension at 10<sup>7</sup> cells/ml in DPBS was serially extruded through polycarbonate membranes filters with 10, 5 and 1 μm of pore sizes (Avanti Polar Lipids). The extruded crude vesicles were filtrated through 0.2 μm of syringe filter (Sartorius, Goettingen, Germany), and CDVs purification was performed using two-step sucrose OptiPrep (Sigma, St. Louis, MO, USA)

density gradient ultracentrifuge. Crude vesicle solution was placed on 10% and 50% OptiPrep density gradient medium and subjected to ultracentrifugation at 100,000  $\times g$  for 2 h at 4 °C. CDVs were obtained from the interface between density gradient and washed with DPBS. CDV pellet was resuspended in DPBS and kept at -80 °C until use.

#### Characterization of CDVs

Size distribution of CDVs was measured by using Zetasizer (Malvern, Worcestershire, UK). CDV purity was evaluated by using UltiMate 3000 UHPLC Systems (Thermo Fisher Scientific, Massachusetts, U.S.A.) equipped with GPC-100 size exclusion column (Eprogen, Illinois, U.S.A.). Particle number of CDVs was measured by nanoparticle tracking analysis (Malvern). The total protein amount in CDVs was measured using bicinchoninic acid (BCA) protein assay kit (Thermo Fisher scientific, MA, USA) after lysis using a radio-immunoprecipitation assay buffer (Thermo Fisher scientific, MA, USA) for 5 min followed by centrifuge at 10,000  $\times g$  for 10 min. Total RNA in CDVs was extracted using TRIzol Reagent (Ambion, Austin, TX, USA).

Cells and CDVs were lysed by RIPA buffer (Thermo Fisher Scientific) and protein concentration was determined by the BCA Protein Assay kit (Thermo Fisher Scientific). Equal amount of protein was separated by SDS-PAGE electrophoresis and transferred to nitrocellulose membranes (Bio-Rad, Berkeley, CA, USA). The nitrocellulose membranes were blocked in 5% (w/v) BSA (Sigma-Aldrich, St. Louis, MO, USA) in 0.2% (v/v) Tween 20 in Tris-buffered saline (Sigma), and then incubated overnight at 4 °C with primary antibody. The primary antibodies used were as follows: mouse monoclonal anti- $\beta$ -Actin antibody (1:1000, Santa Cruz Biotechnology, Inc., Dallas, TX, USA), rabbit monoclonal anti-CD9 antibody (1:2000), rabbit monoclonal anti-CD81 antibody (1:1000, Abcam, Cambridge, UK), and rabbit monoclonal anti-PKR1 antibody (1:1000, Biorbyt, St. Louis, MO, USA). The secondary antibodies used were goat anti-mouse IgG antibody (1:1000) and goat anti-rabbit IgG antibody (1:1000, Thermo Fisher Scientific).

#### RT-PCR

HEK293T cells were treated with 200  $\mu g/ml$  *PROKR1*<sup>Tg</sup> CDVs for 6 h and total RNA was extracted by using a TRIzol reagent (Invitrogen, Carlsbad, CA, USA). About 5  $\mu g$  of total RNAs extracted from HEK293T cells was reverse-transcribed using a reverse transcription kit (Invitrogen) and cDNA was subjected to PCR with *GFP* primer. Human *GAPDH* was used as an internal control. Quantitative measurement of myogenic marker gene expression before and after myogenic differentiation of C2C12 cells was performed using real-time PCR systems with Power SYBR Green PCR Mater Mix (Applied Biosystems, Foster City, CA, USA). The myogenic genes measured were as follows: paired box 3 (*Pax3*), paired box 7 (*Pax7*), and myogenic differentiation 1 (*Myod1*) as early myogenic markers, and myoglobin (*Mb*), myosin heavy chain 7 (*Myh7*), and myoglobin (*Myog*) as late myogenic markers. Data analysis was performed by  $\Delta\Delta Ct$  method using *Gapdh* as a normalizer. Primer information was provided in Supplementary Table 1.

#### Cell uptake of CDVs

*PROKR1*<sup>Tg</sup> CDVs at 100  $\mu g/ml$  were applied to HEK293T cells for 24 h, and real-time uptake process was observed using Cytation 5 (BioTek, Winooski, VT, USA) under GFP channel. The uptake process was capture at every 20 min automatically.

#### Cell viability assay

C2C12<sup>*Prokr1*<sup>-/-</sup></sup> cells at  $1 \times 10^4$  cells/well in 48-well plate (Corning, Corning, NY, USA) were treated with or without *PROKR1*<sup>Tg</sup> CDVs for 48 h. Phenol red-free DMEM media (Thermo Fisher Scientific) were replaced daily. Cell proliferation was measured using an MTT assay kit (Invitrogen, Carlsbad, CA, USA) according to the manufacturer's instruction. Briefly, cells were incubated with 20  $\mu L$  of 12 mM MTT stock solution at 37 °C for 4 h, and 200  $\mu L$  of SDS-HCl solution was added to each well and mix thoroughly. After 4 h, the absorbance was measured by Cytation 5 (BioTek) at 570 nm.

#### Flow cytometry analysis

C2C12<sup>*Prokr1*<sup>-/-</sup></sup> myoblasts were seeded at  $2 \times 10^4$  cells/well of 6-well plate (Corning). *PROKR1*<sup>Tg</sup> CDVs at 25  $\mu g/ml$  were treated to C2C12<sup>*Prokr1*<sup>-/-</sup></sup> myoblast for 3 days. After CDV pretreatment, cells were transferred to the differentiation media without CDVs and incubated for another 3 days. Apoptotic cells after differentiation were measured by flow cytometry (Becton, Dickinson and Company, Franklin Lakes, NJ, USA) with using Alexa Fluor® 488 Annexin V/Dead Cell Apoptosis Kit (Thermo Fisher Scientific, Waltham, MA, USA) at 521 nm and 617 nm.

#### Actin staining

C2C12 cells were seeded on chamber slide (Thermo Fisher Scientific) at  $1 \times 10^4$  cells/slide. After 3 days of CDVs pretreatment and 6 days of myogenic differentiation, myotubes were fixed in 10% (v/v) neutral buffered formalin (Sigma-Aldrich) for 10 min, and then washed with DPBS. Fixed cells were permeabilized with 0.1% (v/v) Triton X-100 (Sigma-Aldrich) for 10 min, and blocked with 2% (w/v) BSA in DPBS for 60 min at room temperature. Cells were then stained with Alexa Fluor® 488 Phalloidin (Thermo Fisher Scientific) for 1 h. After washing with DPBS, cells were counterstained with DAPI (Maravai Life Sciences, San Diego, CA, USA), and the actin fibers were observed in Cytation 5 (BioTek).

#### Glucose uptake assay

Glucose uptake in myotubes was measured using a fluorescent D-glucose analog, 2-[N-(7-nitrobenzene-2-oxa-1,3-diazol-4-yl) amino]-2-deoxy-D glucose (2-NBDG) (Thermo Fisher Scientific). Briefly, myotubes derived from WT C2C12 and C2C12<sup>*Prokr1*<sup>-/-</sup></sup> myoblasts were starved with FBS-free DMEM media for 2 h, and myotubes were stimulated with or without 100 nM insulin (Cell applications, Inc., San Diego, CA, USA) for 30 min. After insulin stimulation, myotubes were treated with 80  $\mu M$  of 2-NBDG for 30 min. Myotubes were washed with cold DPBS, and the fluorescence intensity of the intracellular 2-NBDG was measured at excitation/emission wavelength of 485/535 nm using Cytation 5 (BioTek).

### Biodistribution of CDVs

*PROKR1*<sup>Tg</sup> CDVs were incubated with 5  $\mu$ M XenoLight DiR (PerkinElmer, MA, USA) in 5% (v/v) ethanol at 100 rpm, for 60 min at 37 °C. After incubation, the excess dye was removed by using Zeba Spin<sup>TM</sup> desalting column (Thermo Fisher Scientific). The DiR-labeled CDVs were serially diluted with PBS, and the particle size and number of CDVs were measured by Zeta view (Particle Metrix GmbH, Inning am Ammersee, Germany) before use. Eight-week-old male C57BL/6 mice (Woojung Bio, Inc., Korea) were used for biodistribution experiment ( $N = 3$  per group). Mice were intravenously injected with 150  $\mu$ L of DiR-labeled *PROKR1*<sup>Tg</sup> CDVs at three different dose levels ( $1 \times 10^{11}$  particles/animal as high dose;  $6.8 \times 10^{10}$  particles/animal as medium dose;  $3.2 \times 10^{10}$  particles/animal as low dose). Various organs or tissues including liver, brain, inguinal fat, epididymal fat, gastrocnemius muscle, and soleus muscle were dissected and weighed 6 h post-injection. The intensity of fluorescence of each organ or tissue was quantified using the IVIS Spectrum and Living Image Software (PerkinElmer) to assess the distribution of DiR-labeled *PROKR1*<sup>Tg</sup> CDVs. PBS with DiR only was used as a negative control group to remove the background signal. This study was approved by the Institutional Animal Care and Use Committees of Woojung Bio, Inc. (IACUC2102-016) and was conducted in accordance with the approved guidelines.

### Statistical analyses

Statistics analyses were performed using Prism 8 (GraphPad Software, San Diego, CA, USA). All results were expressed in mean  $\pm$  standard deviation (SD).  $P$  value was calculated using two-sided Student's  $t$  test or one-way ANOVA followed by multiple comparison test for the parametric data, and  $P$  value  $< 0.05$  was considered significant.

## Result

### Generation of genetically engineered cells

*PROKR1*<sup>Tg</sup> HEK293T cells were generated with the piggyBac vector (Figure 1, A) and *PROKR1/Prokr1* knockout cells were prepared using the CRISPR/Cas9 system. To generate *PROKR1*-deficient (*PROKR1*<sup>-/-</sup>) HEK293T cells, a pair of guide RNAs (gRNAs) was used to target the second exon of the *PROKR1* gene, resulting in a deletion of 151 bp (Figure 1, B). To produce *Prokr1*-deficient (*Prokr1*<sup>-/-</sup>) C2C12 cells, another pair of gRNAs was used to target the second exon of the *Prokr1* gene, which produced 26 bp- and 128 bp-deleted homozygous cells (Figure 1, C). All *PROKR1/Prokr1*-engineered cells were subjected to fluorescence-activated cell sorting (FACS) based on the GFP signal and clonal proliferation of the sorted single cell. RT-PCR showed that *PROKR1* mRNA was significantly upregulated in *PROKR1*<sup>Tg</sup> HEK293T cells ( $P < 0.001$ ) compared with the wild-type (WT) counterpart (Figure 1, D). Protein levels of *PROKR1/Prokr1* were significantly upregulated in *PROKR1*<sup>Tg</sup> HEK293T and WT C2C12 cells, and there was no detectable *PROKR1/Prokr1* protein in WT HEK293T, *PROKR1*<sup>-/-</sup> HEK293T, or *Prokr1*<sup>-/-</sup> C2C12 cells (Figure 1, E,

F). These results demonstrated that *PROKR1/Prokr1*-overexpressing and knockout cells were successfully generated; these cells were used as CDV donor and subject cells in subsequent experiments.

### Generation and characterization of CDVs

The preparation of CDVs from genetically engineered HEK293T cells is illustrated in Supplementary Figure 1, A. Following micro-extrusion of  $10^7$  cells through 10-, 5-, and 1- $\mu$ m serial polycarbonate membranes and a 0.2- $\mu$ m filter, crude CDVs were purified by two-step OptiPrep density gradient ultracentrifugation. To verify whether the OptiPrep density gradient ultracentrifuge was effective, CDVs before and after density gradient ultracentrifugation were subjected to size exclusion chromatography analysis. As shown in Supplementary Figure 1, B, CDVs before density gradient ultracentrifugation exhibited peaks at various retention times, while CDVs after density gradient ultracentrifugation exhibited only a single peak at 3.2 min. Thus, OptiPrep density gradient ultracentrifugation appears to be an effective method to obtain highly purified CDVs.

CDVs produced from the genetically engineered HEK293T cells were characterized based on size distribution, exosomal marker expression, particle yield, and the amount of protein and RNA. *PROKR1*<sup>Tg</sup> CDVs had a mean  $\pm$  standard deviation diameter of  $161.7 \pm 12.3$  nm, while *PROKR1*<sup>-/-</sup> CDVs had a mean diameter of  $152.6 \pm 2.9$  nm; there was no significant difference in size distribution between the two types of CDVs (Figure 2, A). Western blotting demonstrated that the two types of CDVs expressed exosomal markers, including CD9 and CD81. In addition, *PROKR1* protein was only detected in *PROKR1*<sup>Tg</sup> cells and CDVs derived from *PROKR1*<sup>Tg</sup> cells, and not in *PROKR1*<sup>-/-</sup> cells or CDVs derived from *PROKR1*<sup>-/-</sup> cells (Figure 2, B). Nanoparticle traffic analysis (NTA) showed that an average of  $6.1 \times 10^{10}$  CDV particles was recovered from  $10^7$  *PROKR1*<sup>Tg</sup> cells while  $6.5 \times 10^{10}$  CDV particles were recovered from the same number of *PROKR1*<sup>-/-</sup> cells; there was no significant difference in the amount of CDVs recovered between the two different sources (Figure 2, C). A total of  $120.5 \pm 20.4$   $\mu$ g of protein was obtained from *PROKR1*<sup>Tg</sup> cell-derived CDVs, while  $87.0 \pm 16.7$   $\mu$ g of protein was obtained from *PROKR1*<sup>-/-</sup> cell-derived CDVs. Furthermore, the total RNA obtained from *PROKR1*<sup>Tg</sup> and *PROKR1*<sup>-/-</sup> CDVs was  $13.7 \pm 2.9$   $\mu$ g and  $10.9 \pm 0.8$   $\mu$ g, respectively; there was no significant difference between these amounts.

RNA quality was compared between donor cells and CDVs, and both showed comparable RNA profiles with small size RNAs at 25 s, 18S ribosomal RNA (rRNA) at 40 s, and 28S rRNA at 47 s; the intensity ratio between 28S rRNA and 18S rRNA was approximately 2:1 (Figure 1, D, E). These results demonstrated that pure CDVs can be prepared from cells with high yield using density gradient ultracentrifugation.

### *PROKR1* delivery to C2C12<sup>Prokr1</sup><sup>-/-</sup> myoblasts

A piggyBac vector expressing GFP simultaneously with *PROKR1* was used to generate HEK293T cells overexpressing *PROKR1*. Tracking of the GFP signal was used to observe the

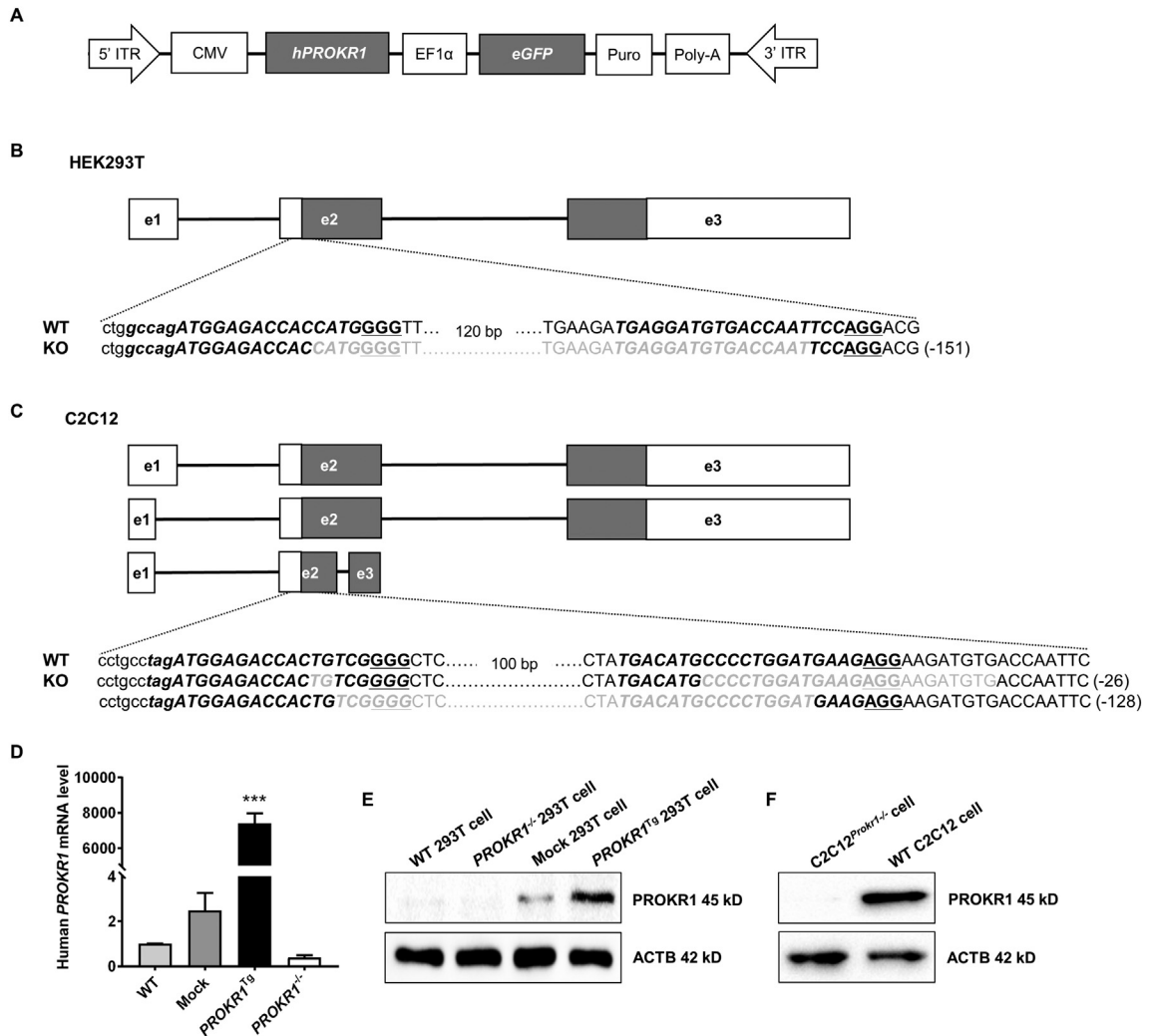


**Figure 1. Generation of *PROKR1/Prokr1* engineered cells.** (A) PiggyBac expression vector construct for human *PROKR1* gene. (B–C) CRISPR/Cas9-mediated *PROKR1/Prokr1* deletion in HEK293T cells and C2C12 cells. Upper characters indicate coding region. Italic characters indicate gRNA binding sites. Underlined characters indicate PAM sequences. Gray characters indicate the deleted sequence in KO cells. The length of deleted sequences is depicted in parenthesis. e = exon. (D) RT-PCR analysis mRNA expression of *PROKR1*. Mock: PiggyBac vector without *PROKR1*. Bars indicate mean  $\pm$  SD, N = 3, \*\*\* $P$  < 0.001 vs. WT, Dunnett's multiple comparison test. (E–F) Western blot analysis of *PROKR1/Prokr1* in HEK293T cells and C2C12 cells. ACTB is used as an internal control.

migration of CDVs to target cells. To verify that CDVs could be internalized by target cells, WT HEK293T cells were treated with 100  $\mu$ g/mL *PROKR1*<sup>Tg</sup> CDVs and the intracellular uptake of CDVs was observed in real time. A GFP signal from *PROKR1*<sup>Tg</sup> CDVs was observed in WT HEK293T cells within 1 h of treatment, and maintained up to 24 h (Figure 3, A). Similarly, GFP mRNA in *PROKR1*<sup>Tg</sup> CDV-treated WT HEK293T cells was detected up to 48 h after treatment (Figure 3, B). These results confirmed that CDVs derived from genetically engineered cells successfully delivered proteins and mRNAs to target cells, and the proteins and mRNAs remained in situ for a prolonged period of time. Based on these results, we investigated whether the membrane protein PROKR1 could be delivered to target cells via CDVs. *Prokr1* knockout C2C12 (C2C12<sup>*Prokr1*<sup>-/-</sup></sup>) myoblasts were treated with CDVs generated from *PROKR1*<sup>Tg</sup> or knockout HEK293T cells, and total protein

was harvested from myoblasts after trypsinization. Western blotting showed that PROKR1 protein was expressed in WT C2C12 and *PROKR1*<sup>Tg</sup> CDV-treated C2C12<sup>*Prokr1*<sup>-/-</sup></sup> cells, while no PROKR1 expression was detected in C2C12<sup>*Prokr1*<sup>-/-</sup></sup> or *PROKR1*<sup>-/-</sup> CDV-treated C2C12<sup>*Prokr1*<sup>-/-</sup></sup> cells (Figure 3, C). Therefore, it was confirmed that both GFP and the membrane protein PROKR1 were delivered to target cells via CDVs. We then determined the optimal concentration of *PROKR1*<sup>Tg</sup> CDVs for cell treatment. C2C12<sup>*Prokr1*<sup>-/-</sup></sup> myoblasts were treated with CDVs at concentrations ranging from 10 to 200  $\mu$ g/mL for 72 h. A cell proliferation assay revealed that CDVs at 50  $\mu$ g/mL or less did not affect cell viability, while CDVs at more than 100  $\mu$ g/mL reduced the number of cells significantly ( $P$  < 0.001) compared to the vehicle control (Figure 3, D). Based on these results, 25  $\mu$ g/mL *PROKR1*<sup>Tg</sup> CDVs was used to induce myogenic effects in C2C12<sup>*Prokr1*<sup>-/-</sup></sup> myoblasts.

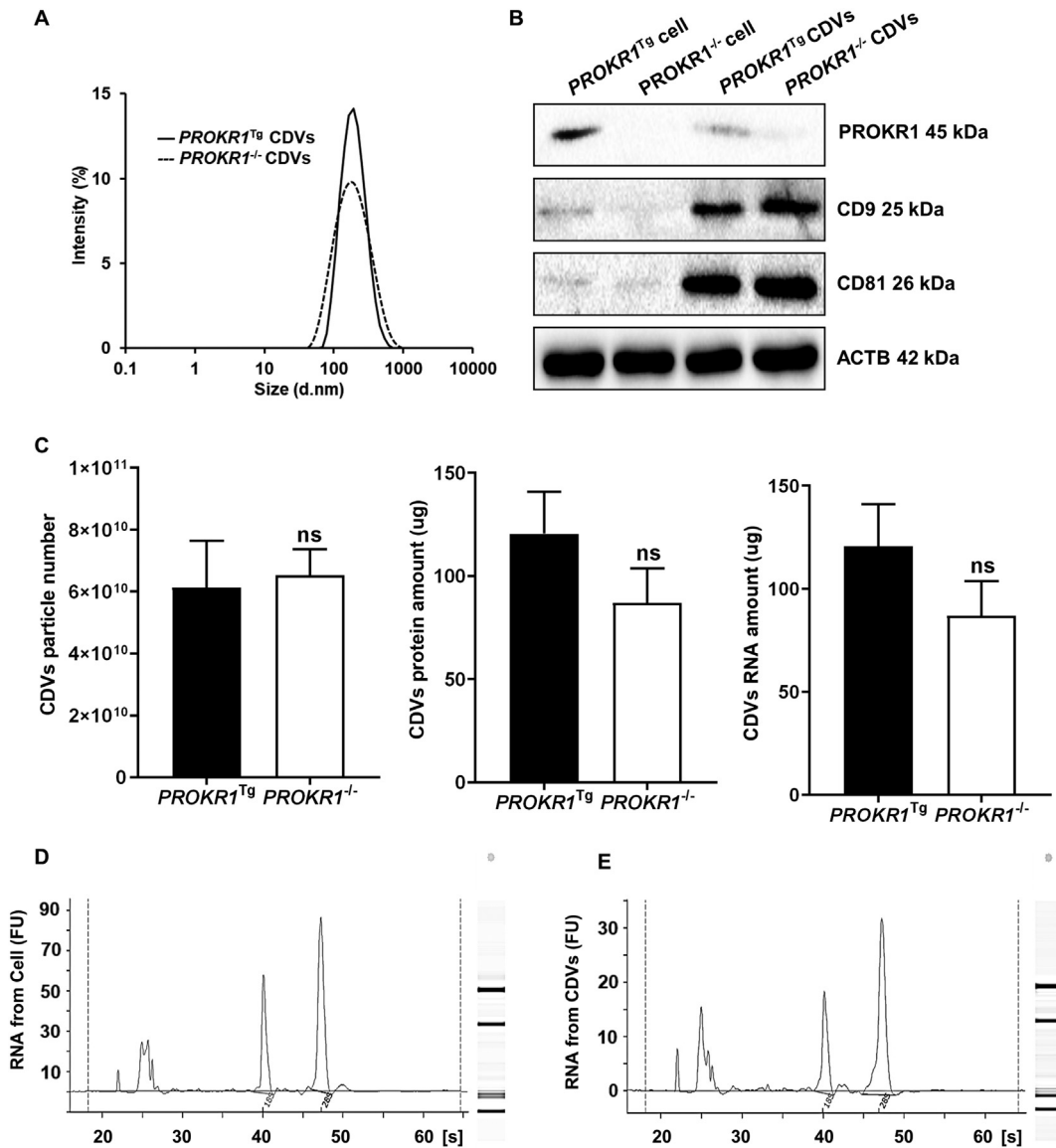


**Figure 2. Characterization of CDVs from genetically engineered HEK293T cells.** (A) Size measurement of CDVs by dynamic light scattering analysis. Solid line indicates the size distribution of *PROKR1*<sup>Tg</sup> CDVs and dotted line indicates the size distribution of *PROKR1*<sup>-/-</sup> CDVs. The line represents the average of the independent triplicate measurements. Horizontal axis indicates the diameter of CDVs (nm); vertical axis indicates the intensity of CDVs (%). (B) Western blot analyses of exosomal proteins and PROKR1 expression in *PROKR1*<sup>Tg</sup> and *PROKR1*<sup>-/-</sup> cells and CDVs. Beta actin (ACTB) is used as an internal control. (C) Quantification of CDV particles, protein, and total RNA in *PROKR1*<sup>Tg</sup> and *PROKR1*<sup>-/-</sup> CDVs. Bars indicate mean  $\pm$  SD,  $N = 3$ . ns: not significant vs. CDVs from *PROKR1*<sup>-/-</sup> HEK293T cells, two-sided Student's *t* test. (D) RNA profile in *PROKR1*<sup>Tg</sup> HEK293T cells. Left panel: chromatogram of different types of RNAs. (E) RNA profile in *PROKR1*<sup>Tg</sup> CDVs. Horizontal axis represents retention time (s), and vertical axis represents the fluorescence unit (FU). Right panel: electrophoresis of different type of RNAs.

#### Anti-apoptotic effects of *PROKR1*<sub>Tg</sub> CDVs in *C2C12*<sup>*Prokr1*<sup>-/-</sup></sup> myocytes

Myotube formation was induced in C2C12 cells with different genotypes. Following differentiation, WT C2C12 cells committed to the myocyte lineage, while *C2C12*<sup>*Prokr1*<sup>-/-</sup></sup> cells showed deleterious morphological changes, eventually detached from the tissue culture plate on differentiation day 3. We then evaluated whether PROKR1 delivered by CDVs could rescue the differentiation potency of *C2C12*<sup>*Prokr1*<sup>-/-</sup></sup> cells.

*C2C12*<sup>*Prokr1*<sup>-/-</sup></sup> myoblasts were treated with CDVs prior to myogenic differentiation for 3 days, and *C2C12*<sup>*Prokr1*<sup>-/-</sup></sup> myocytes treated with *PROKR1*<sub>Tg</sub> CDVs survived 3 days of myogenic differentiation, which was not observed in *PROKR1*<sup>-/-</sup> CDV-treated *C2C12*<sup>*Prokr1*<sup>-/-</sup></sup> cells (Figure 4, A). To determine whether the cellular changes were a result of apoptosis, *C2C12*<sup>*Prokr1*<sup>-/-</sup></sup> myocytes treated with CDVs were subjected to flow cytometry after co-staining with annexin-V (ANXA5) and propidium iodide (PI). In DPBS-treated *C2C12*<sup>*Prokr1*<sup>-/-</sup></sup> myocytes, 47.4%  $\pm$  4.3% of cells were determined to be ANXA5-

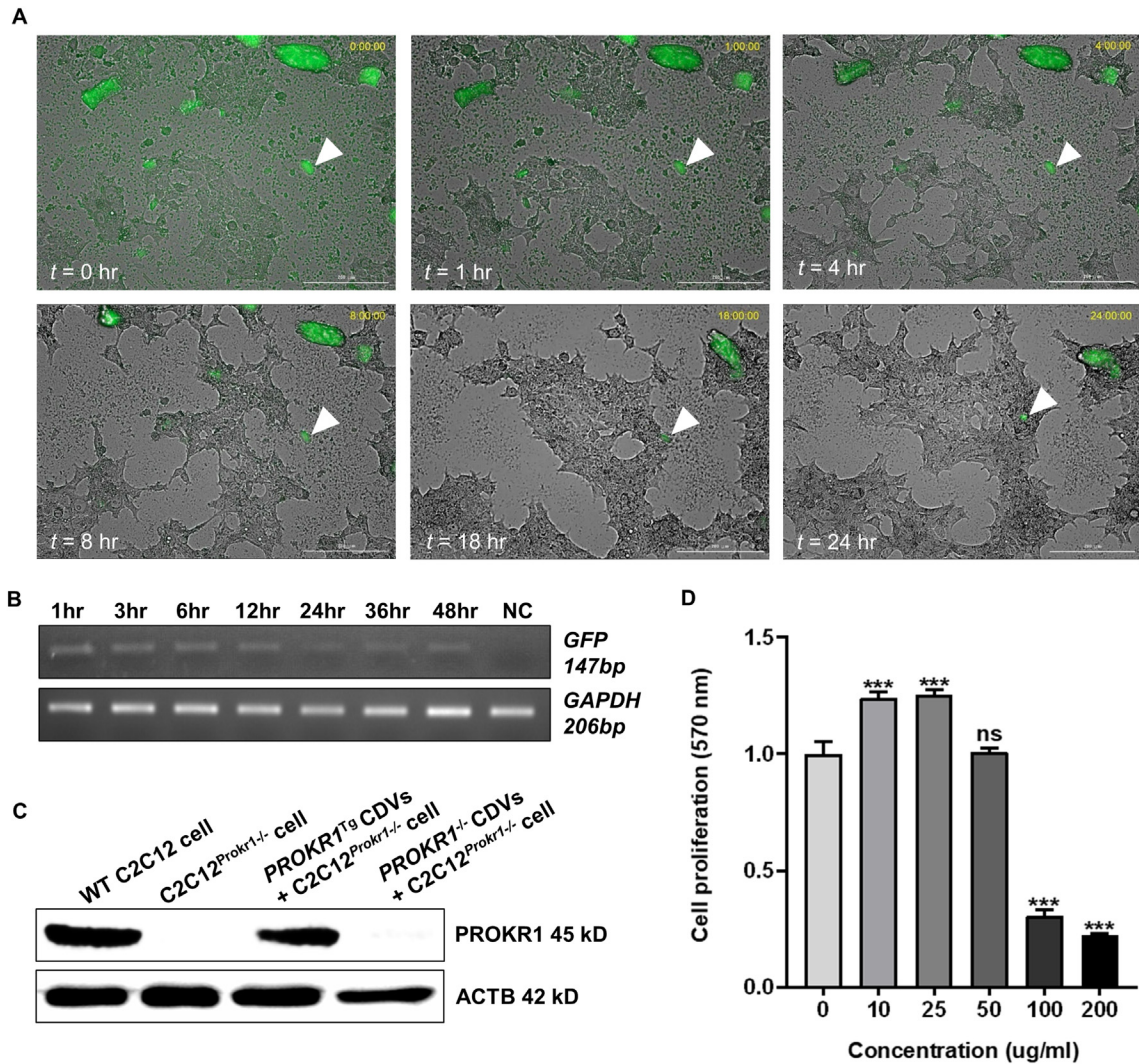


Figure 3. *PROKR1* delivery by *PROKR1*<sup>Tg</sup> CDVs and dose range finding in *C2C12*<sup>Prokr1-/-</sup> myoblasts. (A) Real-time analysis of *PROKR1* protein delivery through *PROKR1*<sup>Tg</sup> CDVs to WT HEK293T cells. Green fluorescence: *PROKR1*<sup>Tg</sup> CDVs contain GFP protein, t: time after CDVs treatment (h), white arrowhead: representative *PROKR1*<sup>Tg</sup> CDVs delivered to naïve cell. Scale bar = 200 μm. (B) RT-PCR analysis of *GFP* mRNA in WT HEK293T after *PROKR1*<sup>Tg</sup> CDVs treatment. NC: WT HEK293T cell control. *GAPDH* is used as an internal control. (C) Western blot analysis of *PROKR1* in *C2C12* myoblasts with or without CDVs treatment. *ACTB* is used as an internal control. (D) MTT assay of *C2C12*<sup>Prokr1-/-</sup> myoblasts treated by various concentration of *PROKR1*<sup>Tg</sup> CDVs. Bars indicate mean ± SD, N = 3. \*\*\**P* < 0.001 vs. 0 μg/mL, Dunnett's multiple comparison test.

positive early apoptotic cells, and 4.1% ± 0.9% were ANXA5/PI-positive late apoptotic cells. By contrast, 36.8% ± 1.9% of *PROKR1*<sup>Tg</sup> CDV-treated *C2C12*<sup>Prokr1-/-</sup> myocytes were in the early apoptotic phase, and 6.3% ± 0.2% were in the late apoptotic phase. A significant reduction of apoptotic cells (8.4%; *P* < 0.05) was seen in *PROKR1*<sup>Tg</sup> CDV-treated *C2C12*<sup>Prokr1-/-</sup> myocytes compared to the DPBS-treated control (Figure 4, B). These results demonstrated that *PROKR1* protein delivered by CDVs ameliorates myogenic commitment-induced apoptosis in *C2C12*<sup>Prokr1-/-</sup> myocytes.

#### Effects of *PROKR1*<sup>Tg</sup> CDVs on *C2C12*<sup>Prokr1-/-</sup> myotube formation and metabolic function

Next, we investigated the recovery of the myogenic potential of *C2C12*<sup>Prokr1-/-</sup> myoblasts by CDV treatment. WT *C2C12* cells differentiated into myofiber-specific F-actin-containing

myotubes after 6 days of myogenic differentiation, and no difference was observed in myotube formation following treatment with *PROKR1*<sup>Tg</sup> or *PROKR1*<sup>-/-</sup> CDVs. In *C2C12*<sup>Prokr1-/-</sup> myoblasts, however, actin fiber-expressing myotubes were not formed after 6 days of myogenic differentiation, consistent with the increased apoptotic cell death. By contrast, pretreatment of *C2C12*<sup>Prokr1-/-</sup> myoblasts with *PROKR1*<sup>Tg</sup> CDVs induced myotubes with F-actin after 6 days of myogenesis. This recovery of myotube formation was not observed in *C2C12*<sup>Prokr1-/-</sup> myoblasts pretreated with *PROKR1*<sup>-/-</sup> CDVs (Figure 5, A).

Gene expression analysis also revealed that myotubes derived from *PROKR1*<sup>Tg</sup> CDV-pretreated *C2C12*<sup>Prokr1-/-</sup> myoblasts had comparable myogenic marker expression to WT myotubes. For example, the expression levels of late myogenic marker genes, including myoglobin (*Mb*), myosin heavy chain 7 (*Myh7*),

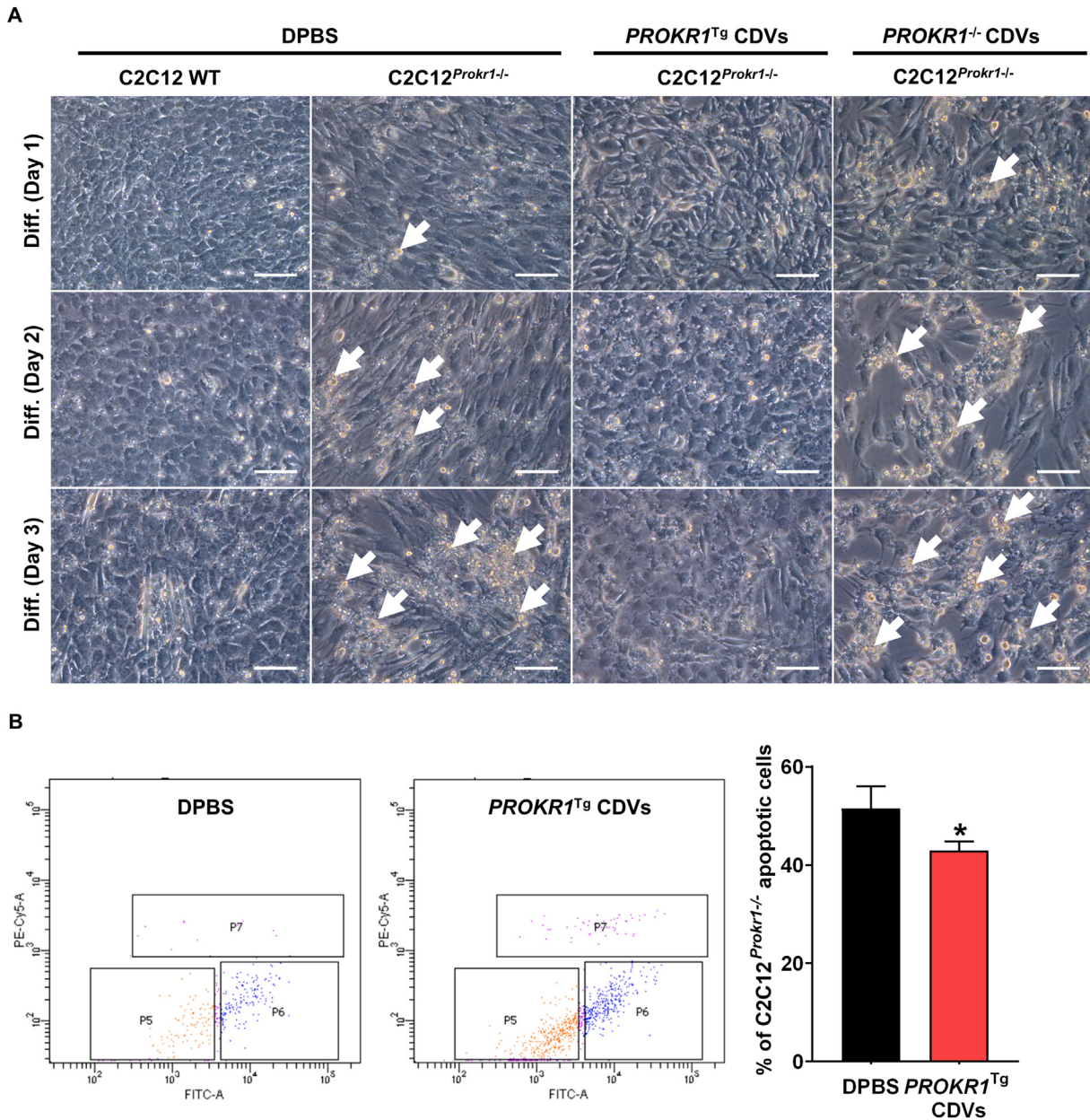


**Figure 4. Anti-apoptotic effect of *PROKR1*<sup>Tg</sup> CDVs on C2C12<sup>Prokr1-/-</sup> myocytes.**(A) Microscopic examination of *PROKR1*<sup>Tg</sup> CDVs-pretreated C2C12<sup>Prokr1-/-</sup> myocytes during myogenic differentiation. Cell morphology on differentiation days 1 to 3 is depicted in a row. White arrows indicate detached cells. Scale bar = 100  $\mu$ m. (B) Flow cytometry analysis of apoptotic C2C12<sup>Prokr1-/-</sup> myoblasts. Left panel: P5 fraction represents live cells, P6 represents ANXA5(+)/PI(-) early apoptotic cells, and P7 (purple) represents ANXA5(+)/PI(-) late apoptotic cells. Right panel: gray bar indicates the percentage (%) of total apoptotic cells in C2C12<sup>Prokr1-/-</sup> myoblast control; black bar indicates the percentage (%) of total apoptotic cells in *PROKR1*<sup>Tg</sup> CDVs-pretreated C2C12<sup>Prokr1-/-</sup> myoblasts. Bars indicate mean  $\pm$  SD,  $N = 3$ . \* $P < 0.05$  vs. DPBS. Two-sided Student's  $t$  test.

and myogenin (*Myog*), in myotubes from both WT C2C12 and *PROKR1*<sup>Tg</sup> CDV-pretreated C2C12<sup>Prokr1-/-</sup> myoblasts increased significantly compared to control myoblasts. Although the expression levels of late myogenic marker genes were significantly different between the two myotubes, treatment with *PROKR1*<sup>Tg</sup> CDVs restored the expression levels such that they were comparable to those of WT myotubes (Figure 5, B). Consistent with these findings, CDV treatment also restored the expression levels of early myogenic marker genes to WT levels. Following myogenic differentiation, early myogenic marker

genes, including paired box 3 (*Pax3*), paired box 7 (*Pax7*), and myogenic differentiation 1 (*Myod1*), were significantly down-regulated in WT C2C12 myotubes. *PROKR1*<sup>Tg</sup> CDV-induced myotubes from C2C12<sup>Prokr1-/-</sup> myoblasts also showed comparable expression levels except for *Myod1*, which was significantly lower by 2 times compared to WT C2C12 myotubes ( $P < 0.0001$ ). However, during myogenesis of C2C12<sup>Prokr1-/-</sup> myoblasts, the expression of early myogenic markers was restored to normal levels by increasing rather than decreasing, which indirectly suggests that a significant error occurred in the

myogenic transcriptional circuit of C2C12 myoblasts due to PROKR1 deficiency.

We then investigated the metabolic function of myotubes induced by *PROKR1*<sup>-/-</sup> CDVs. In WT C2C12 myotubes, insulin-stimulated glucose uptake was significantly increased (by 1.5-fold) compared to the untreated control ( $P < 0.001$ ). However, *PROKR1*<sup>Tg</sup> and *PROKR1*<sup>-/-</sup> CDVs did not increase insulin-stimulated glucose uptake, and there was no synergistic effect with CDVs (Figure 5, C). After myogenic differentiation, insulin treatment did not stimulate glucose uptake in C2C12-*Prokr1*<sup>-/-</sup> myoblasts. By contrast, *PROKR1*<sup>Tg</sup> CDV-induced myotubes showed a significant (1.5-fold) increase in glucose uptake following insulin treatment ( $P < 0.05$ ), to a level equivalent to that of the control. There was no increase in glucose uptake in *PROKR1*<sup>-/-</sup> CDV-induced myotubes following insulin stimulation (Figure 5, D).

Taken together, our results demonstrated that PROKR1 delivered by CDVs promoted the myogenic differentiation of C2C12 myoblasts lacking *Prokr1*, as evidenced by morphological characters and marker expression, while differentiated myotubes acquired normal metabolic function.

#### Biodistribution of *PROKR1*<sup>Tg</sup> CDVs in mice

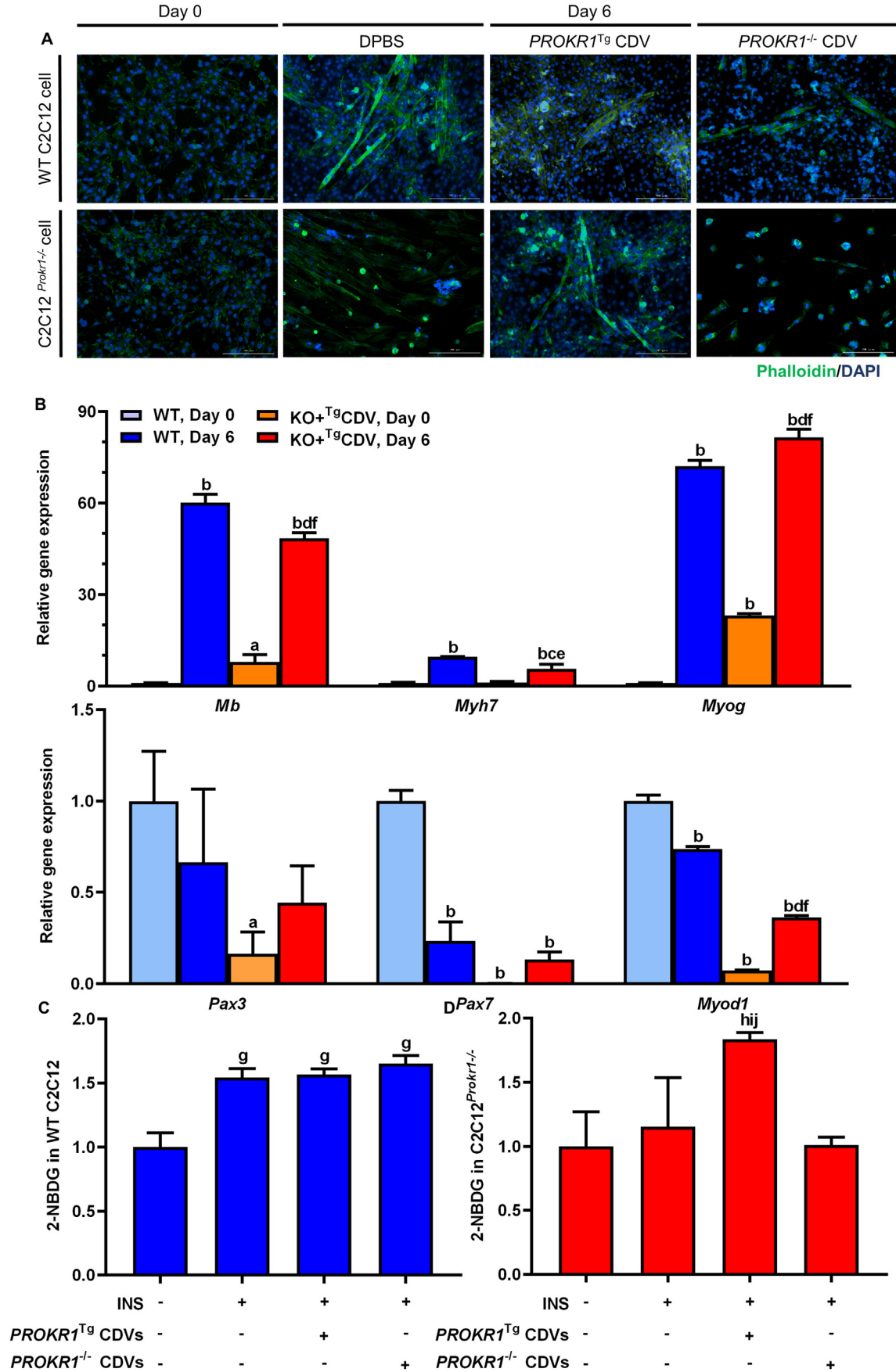
To determine CDV delivery to muscle tissue, we investigated the biodistribution of CDVs by intravenous injection of fluorescence-labeled *PROKR1*<sup>Tg</sup> CDVs at  $3.2 \times 10^{10}$ ,  $6.8 \times 10^{10}$ , or  $1.0 \times 10^{11}$  particles per head in mice as low, medium, or high doses. An increase in fluorescence intensity was observed in a dose-dependent manner in the brain, liver, inguinal fat, epididymal fat, gastrocnemius muscle, and soleus muscle 6 h after injection (Figure 6, A). The average absolute fluorescence intensities in the liver were  $2.9 \times 10^{12}$ ,  $1.9 \times 10^{12}$ , and  $6.6 \times 10^{11}$  [p/s]/[ $\mu\text{W}/\text{cm}^2$ ] at low, medium, and high dose level, and they were at least 5.9 times higher than that of other tissues ( $P < 0.01$ ) (Figure 6, B). The relative fluorescence intensities normalized to organ weight were also highest in the liver in the whole dose levels. However, the average fluorescence intensities in soleus muscle were  $6.6 \times 10^{11}$  and  $7.8 \times 10^{11}$  [p/s]/[ $\mu\text{W}/\text{cm}^2$ ] at medium and high dose levels, respectively, and they were comparable to the relative fluorescence intensities of the liver without significant differences (Figure 6, C). These results indicate that the PROKR1-enriched CDVs could be delivered not only to the liver but also to the muscles, especially to the soleus muscle, which is expected to induce a potential pharmacological effect on improving muscle function and physiology through *PROKR1*<sup>Tg</sup> CDVs.

## Discussion

CDVs have been actively investigated as biotherapeutics and vehicles for drug delivery. The loading efficiency of active pharmaceutical ingredients into vesicles is key for the therapeutic application of CDVs. Since the first attempt to load curcumin into exosomes,<sup>22</sup> incubating exosomes with the drug solution at room temperature has become the most popular method of drug loading, and has improved therapeutic potency.<sup>23</sup> For example, doxorubicin-loaded CDVs exhibited approximately 10-fold

higher drug delivery capacity than free doxorubicin, and reduced tumor growth to the same extent as 20-fold higher doses of the free drug without systemic side effects.<sup>24</sup> Another study compared different techniques for paclitaxel loading into vesicles, including incubation, electroporation, and sonication; loading efficiencies of 1.4%, 5%, and 28%, respectively, were obtained.<sup>25</sup> A small interfering RNA was the first biopharmaceutical loaded into extracellular vesicles (EVs) via electroporation, with 15%-25% efficiency.<sup>26</sup> The loading efficiency and capacity of exosomes for nucleic acids (via electroporation) are limited by the size of the exosome<sup>27</sup>; the loading efficiency of CDVs for nucleic acids has been shown to be superior to that of exosomes.<sup>28</sup> Unlike chemical drugs and nucleic acids, the loading efficiency of exosomes for proteins is limited because proteins have difficulty penetrating cellular membranes and are easily modified by the physiochemical environment.<sup>29</sup> Therefore, various methods and technologies have been developed to deliver proteins to exosomes, including membrane anchoring (XPACK),<sup>30</sup> mechanical dispersion of the membrane by incubation, freeze-thaw, sonication, extrusion,<sup>31</sup> and the optically reversible protein-protein interaction module (EXPLORs).<sup>29</sup> However, there are several limitations of these techniques with respect to enhancing the protein loading efficiency of exosomes. For example, membrane anchoring cannot facilitate intracellular localization of the anchored proteins in target cells, while the efficiency of the mechanical dispersion method depends on the stability of the target protein. In addition, reactivity on optical stimulation differs among the proteins, which limits applicability. Changing the cargo of EVs via genetic modification of cells provides a unique opportunity to enrich the target proteins in EVs. One approach is to transduce cells with a transgene to express the target protein. Exosomes produced from cells overexpressing a reporter protein have been shown to contain abundant protein and were distributed throughout the body.<sup>32,33</sup> In this study, we generated *PROKR1* transgenic HEK293T cells with 9.8-fold higher expression of PROKR1 protein compared to the WT control. CDVs derived from the transgenic cells also contained a comparable amount of protein. In addition, when we applied these CDVs to *Prokr1*-deficient myoblasts, the expression level of PROKR1 recovered to a level similar to that of WT myoblasts, which helped rescue the myogenic potential of *Prokr1*-deficient myoblasts. Although we were unable to quantify the amount of PROKR1 protein contained in CDVs, CDVs produced using transgenic cells demonstrated sufficient target protein loading to induce pharmacological effects.

PROKR1 has been known to regulate angiogenesis, feeding behavior,<sup>34,35</sup> and metabolic disorders. *Prokr1*-deficient mice are obese due to increased proliferation and differentiation of preadipocytes,<sup>17</sup> and exhibit ischemic defects in the heart caused by apoptosis of cardiomyocytes, in turn due to loss of Akt signaling.<sup>36</sup> Akt signaling preserves mitochondrial integrity and function in the heart; a reduction in Akt activity promotes mitochondrial apoptosis. By contrast, activation of Prokr1 signaling prevents doxorubicin-induced apoptosis of cardiomyocytes.<sup>37</sup> However, abnormal phenotypes related to skeletal muscle development and function caused by the loss of *Prokr1* have not yet been reported. Here, we generated



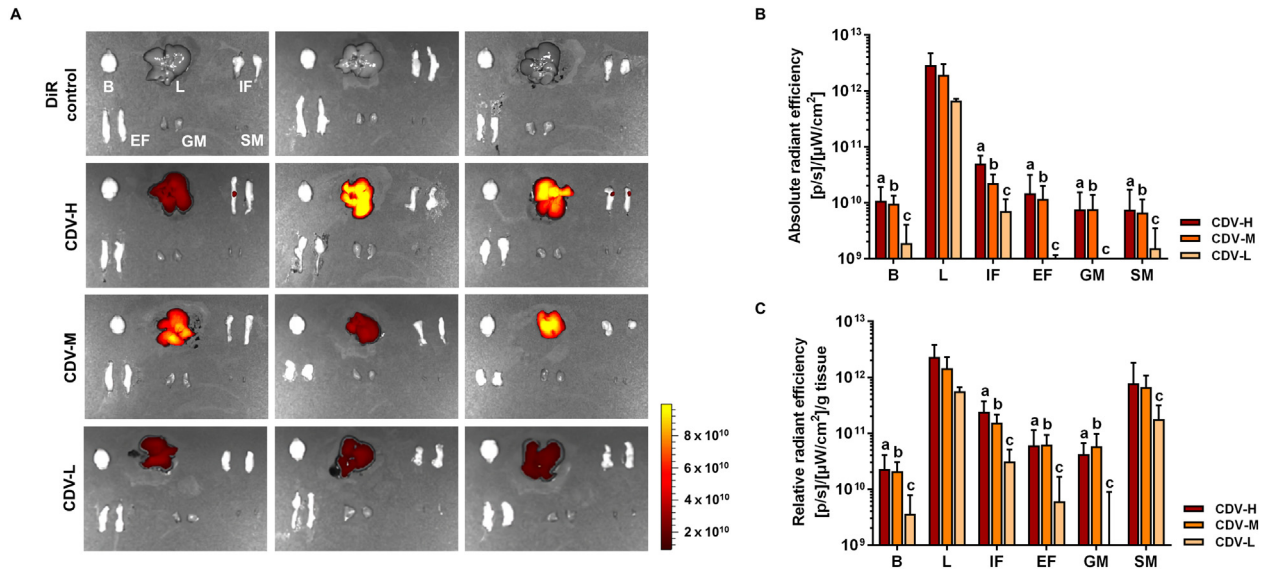


Figure 6. Biodistribution of *PROKR1*<sup>Tg</sup> CDVs in mice. (A) Ex vivo images of brain (B), liver (L), inguinal fat (IF), epididymal fat (EF), gastrocnemius muscle (GM), and soleus muscle (SM) at 6 h post-injection of free DiR and different concentrations of *PROKR1*<sup>Tg</sup> CDVs in mice. Color scale indicates radiant efficiency, min =  $9.15 \times 10^9$ , max =  $9.98 \times 10^{10}$ . (B) Absolute quantification of ex vivo fluorescence in various tissues. Bars indicate mean  $\pm$  SD,  $N = 3$ , <sup>a</sup> $P < 0.01$  vs. liver at high concentration of CDVs (CDV-H), <sup>b</sup> $P < 0.001$  vs. liver at middle concentration of CDVs (CDV-M), <sup>c</sup> $P < 0.001$  vs. liver at low concentration of CDVs (CDV-L). (C) Tissue weight-adjusted relative quantification of ex vivo fluorescence in various tissues. Bars indicate mean  $\pm$  SD,  $N = 3$ , <sup>a</sup> $P < 0.05$  vs. liver at CDV-H, <sup>b</sup> $P < 0.01$  vs. liver at CDV-M, <sup>c</sup> $P < 0.001$  vs. liver at CDV-L.

C2C12<sup>*Prokr1*<sup>-/-</sup></sup> myoblasts; to our knowledge, this is the first report of a loss of myogenic potential of *Prokr1*-deficient myoblasts. The defective myoblasts underwent apoptosis after myogenic commitment. *PROKR1*-enriched CDVs prevented apoptosis of myoblasts and induced myotube formation after myogenic differentiation. Consistent with these findings, *Prokr1* has been shown to play an important role in the differentiation of various cell types. For example, *Prokr1* restores the pluripotency of epicardial-derived progenitor cells, and triggers the differentiation of these cells into endothelial and vascular smooth muscle cells.<sup>38–40</sup> *Prokr1* null mice display a lack of macrophage migration and differentiation.<sup>39</sup> Furthermore, adipocyte-specific *Prokr1*-deficient mice exhibit abnormal accumulation of abdominal fat, suggesting that *Prokr1* suppresses adipose tissue expansion.<sup>17</sup> Interestingly, in a number of obese patients, the muscle fiber composition has been shown to differ from that of non-obese subjects.<sup>41</sup> C2C12 myoblasts are known to differentiate into fast twitch and glycolytic muscle fibers under conventional differentiation conditions.<sup>42</sup> It is unclear whether *Prokr1* contributes to glycolytic muscle fiber specification, or whether fiber-type selective apoptosis is induced when *Prokr1* activity is abrogated. The previous findings, and those of the present study, suggest that *PROKR1* participates in specification of the cell lineage. However, the precise mechanism underlying

the myogenic control of *PROKR1* is beyond the scope of this study and will therefore be the subject of further research.

CDVs can be prepared in a reproducible and cost-effective way. CDVs also exhibit higher circulation and retention times due to a lower clearance rate. These unique features make CDVs an attractive therapeutic option for disease control via the delivery of active pharmaceutical ingredients. However, several prerequisites must be resolved prior to clinical application of CDVs. For example, our study showed that CDV amounts of 50 μg/mL or below were tolerable, which are equivalent to  $4.8 \times 10^4$  CDV particles per cell. However, CDVs at more than 100 μg/mL, equivalent to  $9.8 \times 10^4$  CDV particles per single cell, induced cytotoxicity. Theoretically, approximately  $1 \times 10^4$  CDV particles can be produced from a single cell by micro-extrusion; therefore, this finding indicated that CDV can be safely tolerated in amounts less than 5-fold the CDV production capacity of cells. As CDVs are enclosed by a lipid bilayer, they induce lipid-induced toxicity,<sup>8,43</sup> which has been shown to impede the transportation of biomaterials through the plasma membrane of recipient cells.<sup>44</sup> Moreover, sphingolipids, which are abundant in the CDV membrane, have been shown to cause necrosis or apoptosis in many cell types.<sup>45</sup> While another group has suggested that nanovesicles from HEK293T cells have minimal toxicity and immunogenic effects in mice,<sup>46</sup>

Figure 5. Myogenic effect of *PROKR1*<sup>Tg</sup> CDVs on C2C12<sup>*Prokr1*<sup>-/-</sup></sup> myotubes. (A) Microscopic examination of C2C12<sup>*Prokr1*<sup>-/-</sup></sup> myotubes at day 0 and day 6 of differentiation. Green: Phalloidin staining on actin myofiber, blue: DAPI staining on nuclei. Scale bar = 200 μm. (B) RT-PCR analysis of early and late myogenic marker genes. Bars indicate mean  $\pm$  SD,  $N = 3$ . <sup>a</sup> $P < 0.05$ , <sup>b</sup> $P < 0.001$  vs. WT C2C12 at differentiation day 0 (WT Day 0), <sup>c</sup> $P < 0.01$ , <sup>d</sup> $P < 0.001$  vs. WT day 6, <sup>e</sup> $P < 0.01$ , <sup>f</sup> $P < 0.001$  vs. C2C12<sup>*Prokr1*<sup>-/-</sup></sup> at differentiation day 0 (KO Day 0), Dunnett's multiple comparison test. (C) Insulin-stimulated glucose uptake in WT C2C12 myotubes. (D) Insulin-stimulated glucose uptake in C2C12<sup>*Prokr1*<sup>-/-</sup></sup>-derived myotubes. Bars indicate mean  $\pm$  SD.  $N = 3$ . <sup>g</sup> $P < 0.001$  vs. untreated WT C2C12, <sup>h</sup> $P < 0.01$  vs. untreated C2C12<sup>*Prokr1*<sup>-/-</sup></sup>, <sup>i</sup> $P < 0.05$  vs. insulin (INS)-treated C2C12<sup>*Prokr1*<sup>-/-</sup></sup>, <sup>j</sup> $P < 0.01$  vs. INS + *PROKR1*<sup>-/-</sup> CDVs-treated C2C12<sup>*Prokr1*<sup>-/-</sup></sup>, Dunnett's multiple comparison test.

cytotoxicity of CDVs cannot be ruled out. Moreover, CDV uptake is achieved via ATP-dependent endocytosis, and excessive CDVs would restrict the uptake process.<sup>47</sup> Tissue specificity is another issue for targeted therapeutic delivery using CDVs, because non-specificity of CDV biodistribution might cause unexpected systemic side effects. It is known that exosomes and vesicles preferentially target the cell type from which they were derived.<sup>48,49</sup> Based on these observations, attempts are ongoing to increase the target specificity of CDVs, including target-dependent selection of source cells<sup>50</sup> and surface marker engineering.<sup>32</sup> Transgenesis of source cells is another option to improve the target specificity of CDVs. Quality control during CDV manufacturing will be especially important to meet the regulatory guidelines for drugs and biological products. Industrial quality guidelines for non-clinical and clinical assessment of EV therapeutic products have been issued by the Ministry of Food and Drug Safety of Korea, which requires quality control in terms of the characterization of starting materials; manufacturing method; separation, purification, and characterization of EVs; and stability (<https://nifds.go.kr>). CDVs have not been comprehensively characterized and the extent to which their cargo can be expanded remains to be confirmed. Therefore, establishment of quality control guidelines will promote effective clinical application of CDVs.

In this study, we have demonstrated that CDVs from *PROKRI*<sup>Tg</sup> cells can deliver a target protein to C2C12<sup>Prokr1-/-</sup> myoblasts, reduce apoptotic cell death after myogenic commitment, and rescue the morphological and functional development of myotubes. Furthermore, *PROKRI*<sup>Tg</sup> CDVs were accumulated in soleus muscle comparable to the liver without significant differences. These results provide a basis for further assessment of the potential of engineered CDVs as therapeutic agents. Overall, CDVs appear to be an effective method for delivering active pharmaceutical ingredients and could be used in alternative therapies.

## Appendix A. Supplementary data

Supplementary data to this article can be found online at <https://doi.org/10.1016/j.nano.2021.102448>.

## References

- Colombo M, Raposo G, Thery C. Biogenesis, secretion, and intercellular interactions of exosomes and other extracellular vesicles. *Annu Rev Cell Dev Biol* 2014;**30**:255-89.
- Thery C, Zitvogel L, Amigorena S. Exosomes: composition, biogenesis and function. *Nat Rev Immunol* 2002;**2**(8):569-79.
- Zhuang X, Xiang X, Grizzle W, Sun D, Zhang S, Axtell RC, et al. Treatment of brain inflammatory diseases by delivering exosome encapsulated anti-inflammatory drugs from the nasal region to the brain. *Mol Ther* 2011;**19**(10):1769-79.
- Li P, Kaslan M, Lee SH, Yao J, Gao Z. Progress in exosome isolation techniques. *Theranostics* 2017;**7**(3):789-804.
- Zerlinger E, Barta T, Li M, Vlassov AV. Strategies for isolation of exosomes. *Cold Spring Harb Protoc* 2015;**2015**(4):319-23.
- Ha D, Yang N, Nadithe V. Exosomes as therapeutic drug carriers and delivery vehicles across biological membranes: current perspectives and future challenges. *Acta Pharm Sin B* 2016;**6**(4):287-96.
- Jo W, Kim J, Yoon J, Jeong D, Cho S, Jeong H, et al. Large-scale generation of cell-derived nanovesicles. *Nanoscale* 2014;**6**(20):12056-64.
- Jeong D, Jo W, Yoon J, Kim J, Gianchandani S, Gho YS, et al. Nanovesicles engineered from ES cells for enhanced cell proliferation. *Biomaterials* 2014;**35**(34):9302-10.
- Lunavat TR, Jang SC, Nilsson L, Park HT, Repiska G, Lasser C, et al. RNAi delivery by exosome-mimetic nanovesicles — implications for targeting c-Myc in cancer. *Biomaterials* 2016;**102**:231-8.
- Wu JY, Ji AL, Wang ZX, Qiang GH, Qu Z, Wu JH, et al. Exosome-mimetic nanovesicles from hepatocytes promote hepatocyte proliferation in vitro and liver regeneration in vivo. *Sci Rep* 2018;**8**(1):2471.
- Oh K, Kim SR, Kim DK, Seo MW, Lee C, Lee HM, et al. In vivo differentiation of therapeutic insulin-producing cells from bone marrow cells via extracellular vesicle-mimetic nanovesicles. *ACS Nano* 2015;**9**(12):11718-27.
- Nasiri Kenari A, Kastaniegaard K, Greening DW, Shambrook M, Stensballe A, Cheng L, et al. Proteomic and post-translational modification profiling of exosome-mimetic nanovesicles compared to exosomes. *Proteomics* 2019;**19**(8):e1800161.
- Dawson A, Dennison E. Measuring the musculoskeletal aging phenotype. *Maturitas* 2016;**93**:13-7.
- Cruz-Jentoft AJ, Bahat G, Bauer J, Boirie Y, Bruyere O, Cederholm T, et al. Sarcopenia: revised European consensus on definition and diagnosis. *Age Ageing* 2019;**48**(1):16-31.
- Dennison EM, Sayer AA, Cooper C. Epidemiology of sarcopenia and insight into possible therapeutic targets. *Nat Rev Rheumatol* 2017;**13**(6):340-7.
- Nebigil CG. Prokineticin is a new linker between obesity and cardiovascular diseases. *Front Cardiovasc Med* 2017;**4**:20.
- Szatkowski C, Vallet J, Dormishian M, Messaddeq N, Valet P, Boulberdaa M, et al. Prokineticin receptor 1 as a novel suppressor of preadipocyte proliferation and differentiation to control obesity. *PLoS One* 2013;**8**(12):e81175.
- Kubota T, Kubota N, Kumagai H, Yamaguchi S, Kozono H, Takahashi T, et al. Impaired insulin signaling in endothelial cells reduces insulin-induced glucose uptake by skeletal muscle. *Cell Metab* 2011;**13**(3):294-307.
- Urayama K, Guilini C, Messaddeq N, Hu K, Steenman M, Kurose H, et al. The prokineticin receptor-1 (GPR73) promotes cardiomyocyte survival and angiogenesis. *FASEB J* 2007;**21**(11):2980-93.
- Soga T, Matsumoto S, Oda T, Saito T, Hiyama H, Takasaki J, et al. Molecular cloning and characterization of prokineticin receptors. *Biochim Biophys Acta* 2002;**1579**(2-3):173-9.
- Parker R, Liu M, Eyre HJ, Copeland NG, Gilbert DJ, Crawford J, et al. Y-receptor-like genes GPR72 and GPR73: molecular cloning, genomic organization and assignment to human chromosome 11q21.1 and 2p14 and mouse chromosome 9 and 6. *Biochim Biophys Acta* 2000;**1491**(1-3):369-75.
- Sun D, Zhuang X, Xiang X, Liu Y, Zhang S, Liu C, et al. A novel nanoparticle drug delivery system: the anti-inflammatory activity of curcumin is enhanced when encapsulated in exosomes. *Mol Ther* 2010;**18**(9):1606-14.
- Inamdar S, Nitiyanandan R, Rege K. Emerging applications of exosomes in cancer therapeutics and diagnostics. *Bioeng Transl Med* 2017;**2**(1):70-80.
- Jang SC, Kim OY, Yoon CM, Choi DS, Roh TY, Park J, et al. Bioinspired exosome-mimetic nanovesicles for targeted delivery of chemotherapeutics to malignant tumors. *ACS Nano* 2013;**7**(9):7698-710.
- Kim MS, Haney MJ, Zhao Y, Mahajan V, Deygen I, Klyachko NL, et al. Development of exosome-encapsulated paclitaxel to overcome MDR in cancer cells. *Nanomedicine* 2016;**12**(3):655-64.

- 26 Banizs AB, Huang T, Dryden K, Berr SS, Stone JR, Nakamoto RK, et al. In vitro evaluation of endothelial exosomes as carriers for small interfering ribonucleic acid delivery. *Int J Nanomedicine* 2014;**9**:4223-30.
- 27 Lamichhane TN, Raiker RS, Jay SM. Exogenous DNA loading into extracellular vesicles via electroporation is size-dependent and enables limited gene delivery. *Mol Pharm* 2015;**12**(10):3650-7.
- 28 Vazquez-Rios AJ, Molina-Crespo A, Bouzo BL, Lopez-Lopez R, Moreno-Bueno G, de la Fuente M. Exosome-mimetic nanoplatfoms for targeted cancer drug delivery. *J Nanobiotechnology* 2019;**17**(1):85.
- 29 Yim N, Choi C. Extracellular vesicles as novel carriers for therapeutic molecules. *BMB Rep* 2016;**49**(11):585-6.
- 30 Shen B, Wu N, Yang JM, Gould SJ. Protein targeting to exosomes/microvesicles by plasma membrane anchors. *J Biol Chem* 2011;**286**(16):14383-95.
- 31 Haney MJ, Klyachko NL, Zhao Y, Gupta R, Plotnikova EG, He Z, et al. Exosomes as drug delivery vehicles for Parkinson's disease therapy. *J Control Release* 2015;**207**:18-30.
- 32 Stickney Z, Losacco J, McDevitt S, Zhang Z, Lu B. Development of exosome surface display technology in living human cells. *Biochem Biophys Res Commun* 2016;**472**(1):53-9.
- 33 Mentkowski KI, Snitzer JD, Rusnak S, Lang JK. Therapeutic potential of engineered extracellular vesicles. *AAPS J* 2018;**20**(3):50.
- 34 Dormishian M, Turkeri G, Urayama K, Nguyen TL, Boulberdaa M, Messaddeq N, et al. Prokineticin receptor-1 is a new regulator of endothelial insulin uptake and capillary formation to control insulin sensitivity and cardiovascular and kidney functions. *J Am Heart Assoc* 2013;**2**(5)e000411.
- 35 Beale K, Gardiner JV, Bewick GA, Hostomska K, Patel NA, Hussain SS, et al. Peripheral administration of prokineticin 2 potently reduces food intake and body weight in mice via the brainstem. *Br J Pharmacol* 2013;**168**(2):403-10.
- 36 Boulberdaa M, Turkeri G, Urayama K, Dormishian M, Szatkowski C, Zimmer L, et al. Genetic inactivation of prokineticin receptor-1 leads to heart and kidney disorders. *Arterioscler Thromb Vasc Biol* 2011;**31**(4):842-50.
- 37 Gasser A, Chen Y-W, Audebrand A, Daglayan A, Charavin M, Escoubet B, et al. Prokineticin receptor-1 signaling inhibits dose- and time-dependent anthracycline-induced cardiovascular toxicity via myocardial and vascular protection. *JACC: CardioOncology* 2019;**1**(1):84-102.
- 38 Boulberdaa M, Urayama K, Nebigil CG. Prokineticin receptor 1 (PKR1) signalling in cardiovascular and kidney functions. *Cardiovasc Res* 2011;**92**(2):191-8.
- 39 Urayama K, Guilini C, Turkeri G, Takir S, Kurose H, Messaddeq N, et al. Prokineticin receptor-1 induces neovascularization and epicardial-derived progenitor cell differentiation. *Arterioscler Thromb Vasc Biol* 2008;**28**(5):841-9.
- 40 Cook IH, Evans J, Maldonado-Perez D, Critchley HO, Sales KJ, Jabbour HN. Prokineticin-1 (PROK1) modulates interleukin (IL)-11 expression via prokineticin receptor 1 (PROKR1) and the calcineurin/NFAT signalling pathway. *Mol Hum Reprod* 2010;**16**(3):158-69.
- 41 Tanner CJ, Barakat HA, Dohm GL, Pories WJ, MacDonald KG, Cunningham PR, et al. Muscle fiber type is associated with obesity and weight loss. *Am J Physiol Endocrinol Metab* 2002;**282**(6):E1191-6.
- 42 Lee KY, Singh MK, Ussar S, Wetzel P, Hirshman MF, Goodyear LJ, et al. Tbx15 controls skeletal muscle fibre-type determination and muscle metabolism. *Nat Commun* 2015;**6**:8054.
- 43 Petersen S, Steiniger F, Fischer D, Fahr A, Bunjes H. The physical state of lipid nanoparticles influences their effect on in vitro cell viability. *Eur J Pharm Biopharm* 2011;**79**(1):150-61.
- 44 Zepik HH, Walde P, Kostoryz EL, Code J, Yourtee DM. Lipid vesicles as membrane models for toxicological assessment of xenobiotics. *Crit Rev Toxicol* 2008;**38**(1):1-11.
- 45 Kolesnick RN, Kronke M. Regulation of ceramide production and apoptosis. *Annu Rev Physiol* 1998;**60**:643-65.
- 46 Zhu X, Badawi M, Pomeroy S, Sutaria DS, Xie Z, Baek A, et al. Comprehensive toxicity and immunogenicity studies reveal minimal effects in mice following sustained dosing of extracellular vesicles derived from HEK293T cells. *J Extracell Vesicles* 2017;**6**(1):1324730.
- 47 Ronquist KG, Sanchez C, Dubois L, Chiourea D, Fonseca P, Larsson A, et al. Energy-requiring uptake of prostasomes and PC3 cell-derived exosomes into non-malignant and malignant cells. *J Extracell Vesicles* 2016;**5**:29877.
- 48 Zhu JY, Zheng DW, Zhang MK, Yu WY, Qiu WX, Hu JJ, et al. Preferential cancer cell self-recognition and tumor self-targeting by coating nanoparticles with homotypic cancer cell membranes. *Nano Lett* 2016;**16**(9):5895-901.
- 49 Zhai Y, Su J, Ran W, Zhang P, Yin Q, Zhang Z, et al. Preparation and application of cell membrane-camouflaged nanoparticles for cancer therapy. *Theranostics* 2017;**7**(10):2575-92.
- 50 Snell AA, Neupane KR, McCorkle JR, Fu X, Moonschi FH, Caudill EB, et al. Cell-derived vesicles for in vitro and in vivo targeted therapeutic delivery. *ACS Omega* 2019;**4**(7):12657-64.